CORA Cork Open Research Archive
Cartlann Taighde Oscailte Chorcaí

| | |
|---|---|
| Title | 2 pi steradian coverage transmit-receive lasercom system using smart multiplexing of multiplexed optical scanners |
| Authors | Yaqoob, Zahid;Riza, Nabeel A. |
| Publication date | 2002-12-09 |
| Original Citation | Yaqoob, Z. and Riza, N. A. (2002) '2 pi steradian coverage transmit-receive lasercom system using smart multiplexing of multiplexed optical scanners', Proceedings of SPIE, 4821, Free-Space Laser Communication and Laser Imaging II;International Symposium on Optical Science and Technology Seattle, WA, United States, doi: 10.1117/12.453804 |
| Type of publication | Conference item |
| Link to publisher's version | 10.1117/12.453804 |
| Rights | © 2002 Society of Photo-Optical Instrumentation Engineers (SPIE). One print or electronic copy may be made for personal use only. Systematic reproduction and distribution, duplication of any material in this paper for a fee or for commercial purposes, or modification of the content of the paper are prohibited. |
| Download date | 2025-04-28 04:52:26 |
| Item downloaded from | https://hdl.handle.net/10468/10169 |

UCC
University College Cork, Ireland
Coláiste na hOllscoile Corcaigh

PROCEEDINGS OF SPIE

SPIEDigitalLibrary.org/conference-proceedings-of-spie

# Two-pi steradian coverage transmit-receive lasercom system using smart multiplexing of multiplexed optical scanners

Yaqoob, Zahid, Riza, Nabeel

Zahid Yaqoob, Nabeel A. Riza, "Two-pi steradian coverage transmit-receive lasercom system using smart multiplexing of multiplexed optical scanners," Proc. SPIE 4821, Free-Space Laser Communication and Laser Imaging II, (9 December 2002); doi: 10.1117/12.453804

SPIE.

Event: International Symposium on Optical Science and Technology, 2002, Seattle, WA, United States

Downloaded From: https://www.spiedigitallibrary.org/conference-proceedings-of-spie on 07 Jun 2020 Terms of Use: https://www.spiedigitallibrary.org/terms-of-use

# 2π Steradian Coverage Transmit-Receive Lasercom System using Smart Multiplexing of Multiplexed Optical Scanners

Zahid Yaqoob and Nabeel A. Riza*

Photonic Information Processing Systems (PIPS) Laboratory
The School of Optics/Center for Research and Education in Optics and Lasers (CREOL)
University of Central Florida, 4000 Central Florida Blvd, Orlando, FL 32816-2700
Tel: 407-823-6829; Fax: 407-823-6880
E-mail: riza@creol.ucf.edu

## ABSTRACT

Wide area (such as 2π steradian) coverage transmit-receive lasercom sub-system is proposed. The lasercom sub-system design utilizes recently proposed new beam scanning approach called Multiplexed Optical Scanner Technology (MOST) that promises high-speed reconfiguration, low power consumption, large aperture, and wide coverage desired for agile, low cost, and easy to install free-space optical link system. The stringent sub-system goals are met by introducing the concept of "Multiplexing" at both the *scanner interconnection level* and the *light property level*. The scanner interconnections can be parallel or serial or both. The light properties that can be multiplexed include polarization, time, wavelength, space, and spatial codes. Manipulating the mentioned parameters of light, various multiplexed optical scanners (MOSs) can be realized. The highly sought after lasercom sub-system design will consist of two or more MOSs combined together in a smart fashion.

## 1. INTRODUCTION

An optical beam scanner with no-moving parts, wide angular scan range, large diameter aperture, and microsecond domain scan setting speeds is desired in many applications such as laser ultrasonics and free-space laser communications. Previous technologies such as acousto-optics[1], electro-optics[2], microelectromechanical systems[3], and opto-mechanics[4] have been hard pressed in realizing these scanner goals. Recently, we have proposed a new approach called Multiplexed Optical Scanner Technology (MOST) to realize the highly sought after lasercom sub-system design.[5] MOST features true rapid 3-D beamforming to accurately control the beam position, power and shape, all at microsecond or less switching time. The stringent sub-system goals are met by introducing the concept of "Multiplexing" at both the *scanner interconnection level* and the *light property level*. The scanner interconnections can be parallel or serial or both. The light properties that can be multiplexed include polarization, time, wavelength, space, and spatial codes. Manipulating the mentioned parameters of light, various multiplexed optical scanners (MOSs); namely, polarization (P)-MOS, time (T)-MOS, wavelength (W)-MOS, space (S)-MOS, and spatial code (C)-MOS can be realized. In this paper, we will first highlight the individual scanners in the MOST family (i.e., W-MOS and P-MOS) which will be used to design the lasercom sub-system. We will explain the design and assembly of our hand-held free-space W-MOS unit and discuss smart scanner modules that will be used to design an agile lasercom sub-system with an unprecedented 360° azimuthal coverage and fine (e.g., ± 5°) elevation scans. In addition, we will also describe how the proposed smart multiplexing of MOSs can be extended to realize an eye-safe transmit-receive lasercom sub-system with 2π steradian coverage for military mobile ground, air, and sea platforms.

The wavelength-multiplexed optical scanner (W-MOS) is a peer member of the MOST family. The scanner gets its power from high speed wavelength selection coupled with light interaction with a wavelength dispersive element that in turn leads to spatially dispersed beam scanning. There are two key versions of the W-MOS; namely, the free-space W-MOS and the fiber-remoted W-MOS. The fiber-remoted version can provide a scanner field of view as

* Also with Nuonics Inc., Orlando FL; www.nuonics.com



Free-Space Laser Communication and Laser Imaging II, Jennifer C. Ricklin, David G. Voelz, Editors, Proceedings of SPIE Vol. 4821 (2002) © 2002 SPIE · 0277-786X/02/$15.00

Downloaded From: https://www.spiedigitallibrary.org/conference-proceedings-of-spie on 07 Jun 2020
Terms of Use: https://www.spiedigitallibrary.org/terms-of-use

large as 360° and gives the powerful ability to scan large volumes and complicated three-dimensional (3-D) geometries.[6] We have completed the theoretical analysis of free-space W-MOS [7] and have demonstrated high resolution (≤1 mrad for a 1.875 cm diffraction limited aperture diameter) and large angular scans (~13°).[8] The potential speed of W-MOS can be in GHz using the present-day state-of-the-art nanosecond tuning speed lasers.[9] The polarization-multiplexed optical scanner (P-MOS) uses a binary switched serial beam control architecture with polarization multiplexing that results in an N-bit cascaded 3-D beamforming control architecture.[10] The P-MOS uses single pixel 90° linear polarization rotators such as ferroelectric liquid crystal (FLC) cells to act as the electrically-controlled polarization multiplexing components. The 3-D beamforming information such as tilt, focus, and defocus are stored in large area birefringent phase plates. These phase plates can be electronically programmable single pixel thin film devices. For $2^N$ independent 3-D beam patterns, N binary FLC cells and N birefringent phase plates are required.

## 2. HAND-HELD FREE-SPACE W-MOS DESIGN AND ASSEMBLY

Figure 1 (a) shows the basic structure of the free-space W-MOS design with single beam high-speed one-dimensional (1-D) scanning capability where the wavelength selection is achieved by tuning a laser or via a tunable optical filter such as an acousto-optic tunable filter. In both cases, very high-speed beam scanning can be achieved using electronically tuned solid state lasers[11, 12] and filters.[13-15]

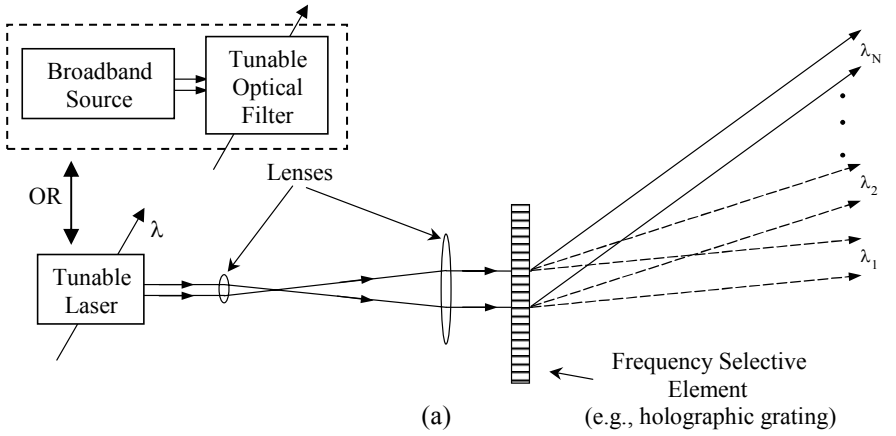


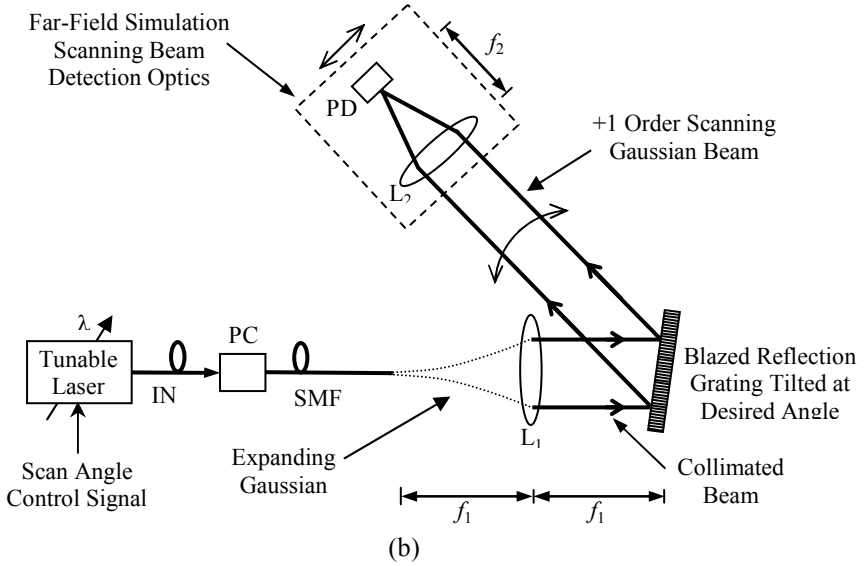


Fig. 1 shows (a) the basic design of free-space W-MOS for implementing no moving parts high speed one dimensional (1-D) scans and (b) the schematic for our hand-held free-space W-MOS.



Downloaded From: https://www.spiedigitallibrary.org/conference-proceedings-of-spie on 07 Jun 2020
Terms of Use: https://www.spiedigitallibrary.org/terms-of-use

Figure 1 (b) shows the schematic for our hand-held frees-space W-MOS. Light from the tunable laser is coupled into a fiber-coupled PC that is used to adjust the polarization of the incident beam for optimized scanner insertion loss. After the PC, the light couples into a single mode fiber (SMF) that terminates in a receptacle style fiber collimator. The collimator consists of an assembly that aligns the SMF with the optical axis of lens $L_1$ and keeps the polished end of the SMF at one focal length distance from an achromatic lens ($f_1$ = 45 mm) to get a collimated Gaussian beam with 8.3 mm $1/e^2$ beam size. The incident collimated beam hits the grating at an angle $\theta_{inc}$ and the $m^{th}$ order beam is deflected in the direction $\theta(m)$ given by [7]

$$\theta(m) = \sin^{-1}\left\{\frac{m\lambda}{L} + \sin\theta_{inc}\right\}, \qquad (1)$$

where $\lambda$ is the wavelength of the incident beam and $L$ is the period of the grating. Figure 2 shows the assembly of the hand-held free-space W-MOS unit. All the opto-mechanical parts of the scanner are mounted on an aluminum base plate **1**. The receptacle style fiber collimator **2** that uses an aspheric lens is fixed on the base plate using an aluminum holder **3**.

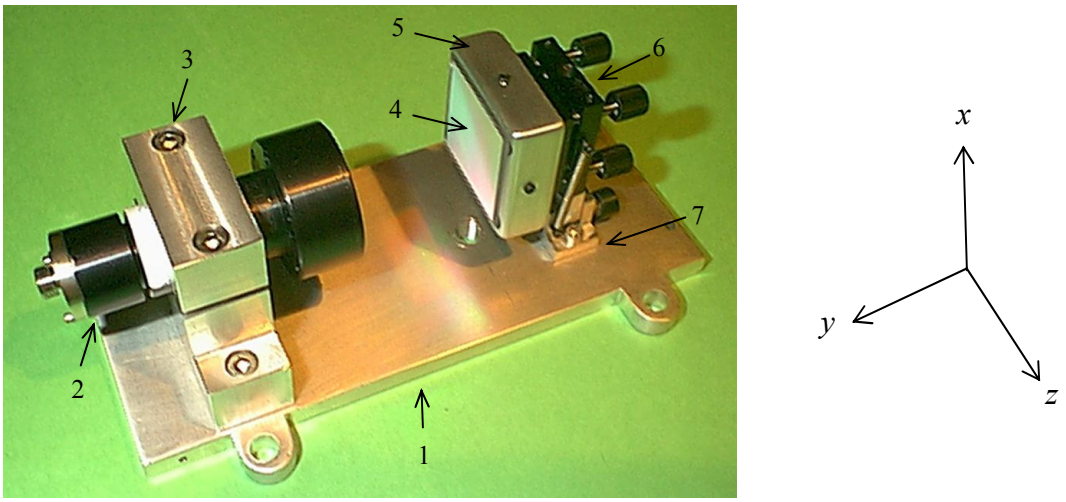


Fig. 2 Assembly of the handheld W-MOS unit. 1: Aluminum base plate; 2: Receptacle style fiber collimator; 3: Fiber collimator holder; 4: Blazed reflection grating; 5: Grating holder; 6: Tip-tilt stage for tilts in *xy* and *yz*-plane; 7: Aluminum stage for tilts in *xz*-plane.

A blazed reflection grating **4** (grating period $L$ = 1/600 mm) is mounted on the other end of the base plate. The grating mount consists of a grating holder, a 2-D tip-tilt stage, and a 1-D tilt stage marked as **5**, **6**, and **7**, respectively. The grating holder is attached to the tip-tilt stage **6** and has two set screws (one at the top and the other on one side) to hold the grating. The tip-tilt stage **6** adjusts the tilt of the blazed grating in *xy* and *yz*-planes. Furthermore, the non-tilting back plane of the tip-tilt stage **6** is attached to an aluminum 1-D tilt stage **7** designed to adjust grating vector's tilt in the *xz*-plane. The hand-held W-MOS unit was assembled as shown in Fig. 2. The tip-tilt stage **6** was used to set the angle of incidence $\theta_{inc} \sim 2.2^o$. By changing the wavelength via electronic control of the tunable source, the light output from the hand-held W-MOS moves spatially in the *yz*-plane, creating an array of optical dots in space.

The hand-held W-MOS assembly is mounted on a test setup (see Fig. 3). The scanning +1 diffraction order is tracked with the help of beam detection optics (a focusing lens at one focal length distance from a photodetector) mounted on an aluminum C-channel with one end attached to a rotational stage having the same axis of rotation as that of the reflection grating. A fiber-coupled mechanically tuned laser with an 80 nm tunable bandwidth centered at 1560 nm is used as the tunable light source. A SMF patch cord (FC/APC - FC/PC) connects the tunable laser with the W-MOS unit. Note that the FC/PC end of the patch cord goes into the hand-held W-MOS unit.



Downloaded From: https://www.spiedigitallibrary.org/conference-proceedings-of-spie on 07 Jun 2020
Terms of Use: https://www.spiedigitallibrary.org/terms-of-use

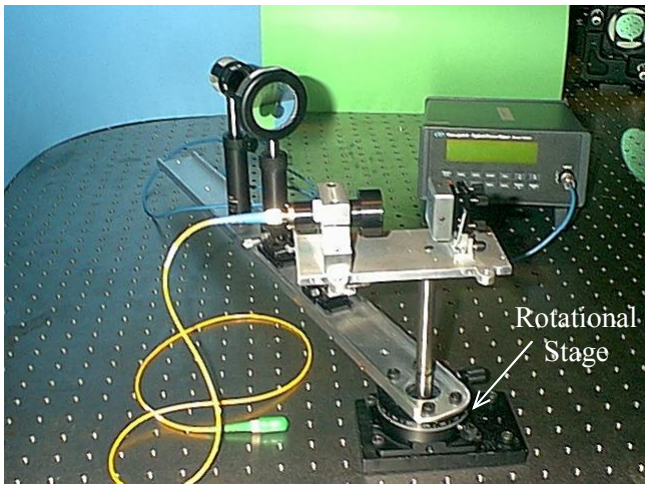


Fig. 3 Setup to measure the deflection angle, diffraction efficiency, and the beam profile of the diffracted +1 order beam.

Figure 4 (a) shows both the measured as well as theoretical angular scan plots versus wavelength of the tunable laser. A total angular scan of 14.99$^o$ is achieved which is in complete agreement with the theoretical angular scan of 14.97$^o$ (available for $\theta_{inc}$ = 2.207$^o$) as the wavelength of the source is tuned from 1520 nm to 1600 nm. The insertion loss (IL) of the hand-held W-MOS unit was also studied. The IL of the W-MOS is directly related to the design and diffraction efficiency (DE) of the grating used in the setup. The DE of a grating is defined as the fraction of incident monochromatic light diffracted into a specific order. To study the insertion loss of the laboratory W-MOS, the power in the scanning +1 diffracted beam is measured versus the wavelength of the tunable source. The results shown in Fig. 4 (b) indicate that the insertion loss of the W-MOS unit increases as the wavelength of tunable source is increased.

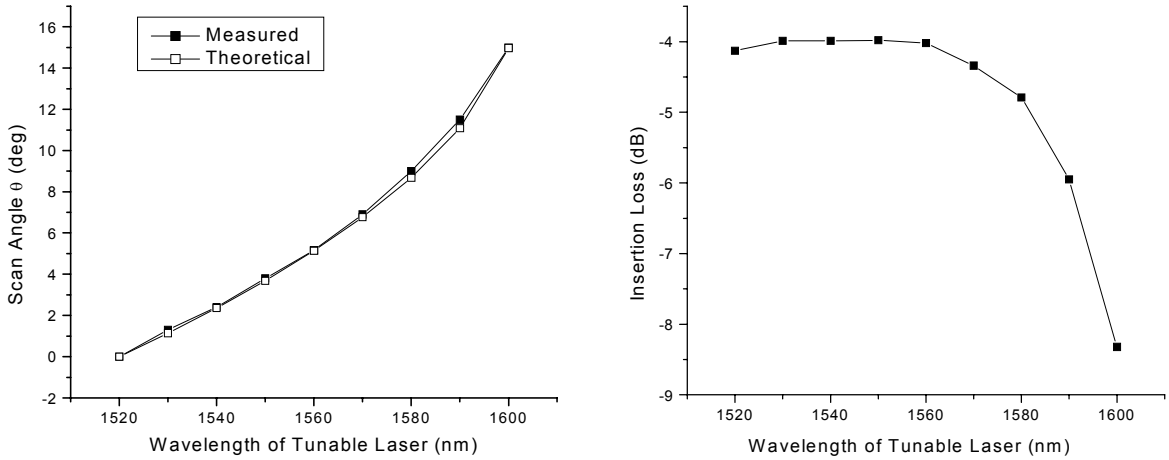


Fig. 4 shows (a) angular scan range and (b) the Insertion loss, respectively, of the hand-held W-MOS unit versus wavelength of the tunable laser

Another important parameter studied is the quality of the scanning diffracted beams. To start with, we first measured the beam quality of the incident beam for both 1520 nm and 1600 nm. Knife-edge method was used to study the beam profile in both horizontal and vertical directions. Figure 5 shows the incident beam profiles for 1520 nm and 1600 nm. It can be seen that 1/e$^2$ beam size (2$w$) for all cases is ~ 8.6 mm. Note that for each case, the data was fit with the following expression to determine the Gaussian beam waist and hence the 1/e$^2$ beam diameter

$$y = y_0 + \frac{P_0}{2} erf\left\{\frac{x - x_0}{w_0}\right\}, \qquad (2)$$



Downloaded From: https://www.spiedigitallibrary.org/conference-proceedings-of-spie on 07 Jun 2020
Terms of Use: https://www.spiedigitallibrary.org/terms-of-use

where,

$$erf(x) = \frac{2}{\pi}\int_0^x e^{-t^2}\,dt\,. \tag{3}$$

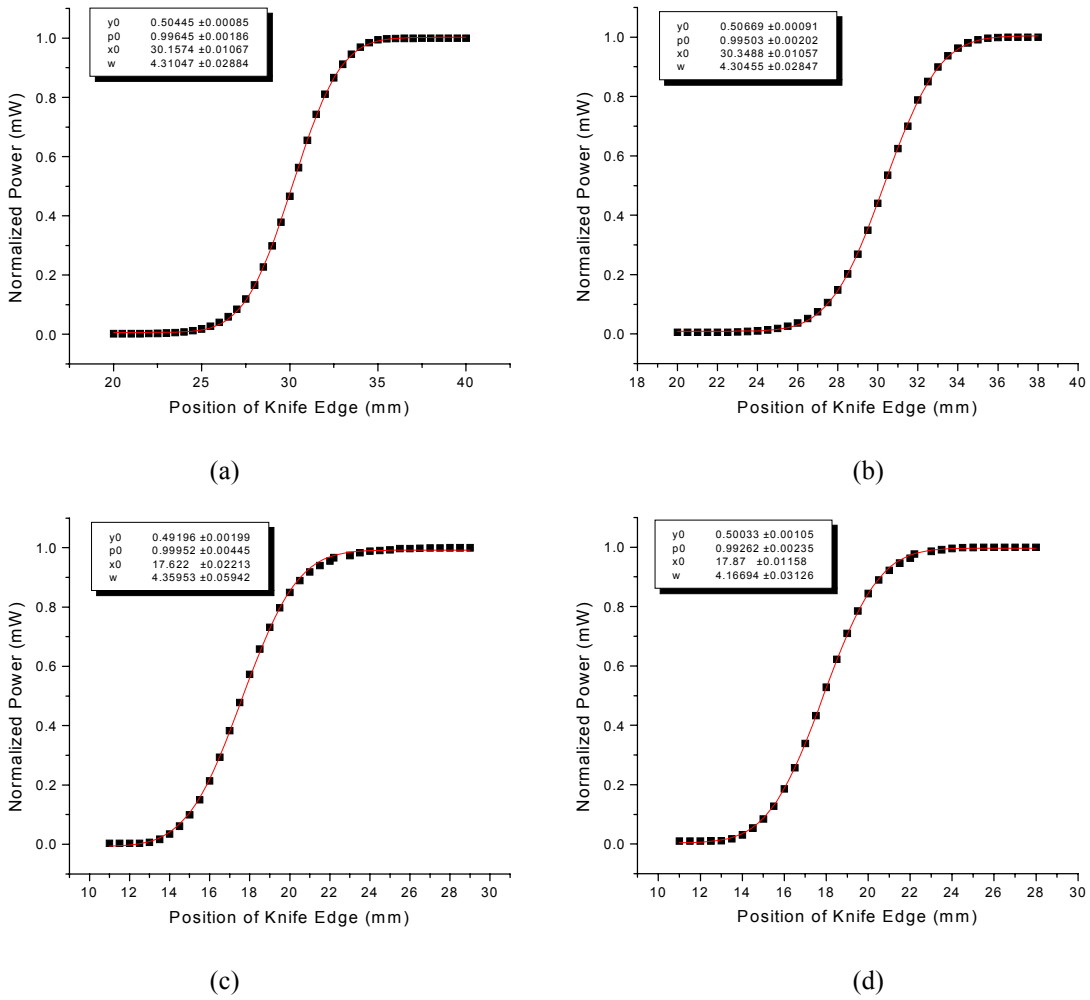


Fig. 5 (a) and (b) show the horizontal beam profiles of incident beam for 1520 nm and 1600 nm, respectively, whereas (c) and (d) indicate the vertical beam profiles of incident beam for 1520 nm and 1600 nm, respectively.

After the beam profile of the incident beam had been measured, we also studied the quality of the diffracted beams at 17 cm from the grating center. Figure 6 shows the vertical beam profiles of the diffracted beams for 1520 nm and 1600 nm. As expected, the $1/e^2$ vertical beam diameter remains same as that of the incident beam, i.e., 8.6 mm. On the other hand, the $1/e^2$ horizontal beam diameter decreases as the wavelength of the tunable laser is increased from 1520 nm to 1600 nm as suggested by [7]

$$w(r_0) = w_{\text{eff}}\sqrt{1+\left(\frac{r_0}{z_0}\right)^2}\,, \tag{4}$$

where $r_0$ is the distance between the grating and knife-edge plane and $z_0$ is given by [7]

$$z_0 = \frac{\pi w_{\text{eff}}^2}{\lambda}\,. \tag{5}$$



Downloaded From: https://www.spiedigitallibrary.org/conference-proceedings-of-spie on 07 Jun 2020
Terms of Use: https://www.spiedigitallibrary.org/terms-of-use

Note that $w_{\text{eff}}$ is the effective beam waist of the diffracted beam and is related to the incident beam waist $w_{\text{inc}}$ through the following expression [7]

$$w_{\text{eff}} = w_{\text{inc}} \frac{\cos\theta(m)}{\cos\theta_{\text{inc}}}. \quad (6)$$

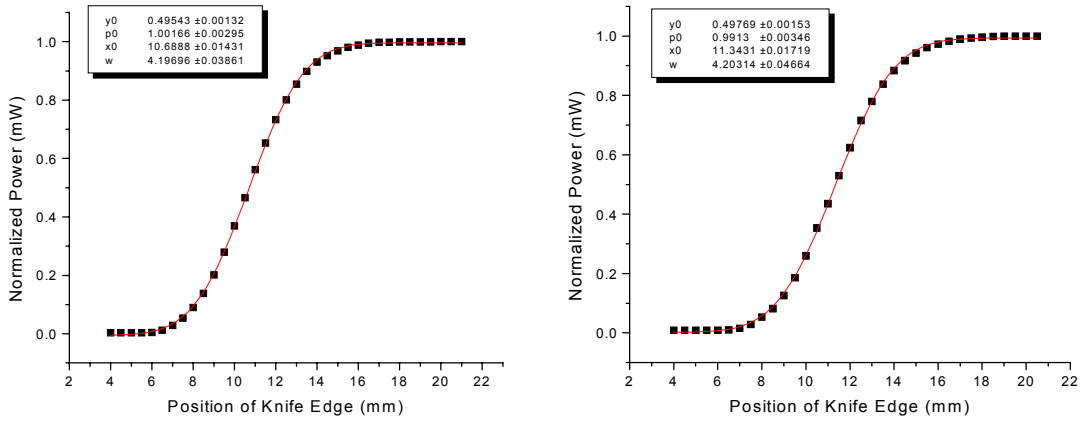


(a) (b)

Fig.6 shows the vertical beam profiles of the diffracted beam for (a) 1520 nm and (b) 1600 nm.

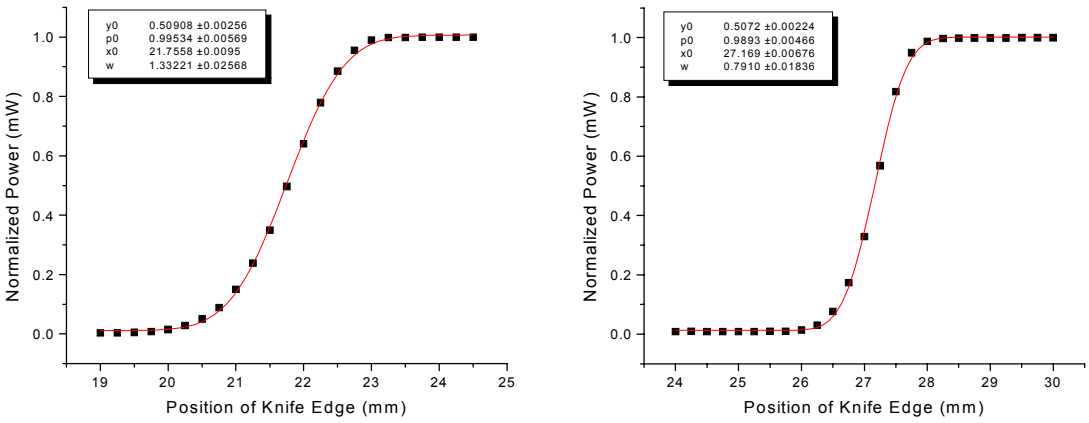


(a) (b)

Fig. 7 shows the horizontal beam profiles of the diffracted beam for (a) 1520 nm and (b) 1600 nm.

As shown in Fig. 7, the $1/e^2$ horizontal beam waists are measured as 1.33 mm and 0.79 mm at 1520 nm and 1600 nm, respectively. Note that the theoretical $1/e^2$ horizontal beam diameters calculated using Eqs. (5), (6), and (7) are 1.34 mm and 0.69 mm at 1520 nm and 1600 nm, respectively.

In conclusion, the hand-held W-MOS unit provides an angular scan of 14.99°. The insertion loss of the scanner increases as the wavelength of tunable source is increased. Note that if the wavelength is not increased beyond 1580 nm, the insertion loss numbers are pretty reasonable [see Fig. 4 (b)]. However by doing so, the total available angular scan range will reduce to 8.68°. This indicates that there is a trade-off between the insertion loss and angular scan range of our hand-held W-MOS unit. Also note that the scanner insertion loss profile versus wavelength of tunable source will be different for different angles of incidence. For example, the blazed grating gives best DE (and hence lowest scanner insertion loss) when used in Littrow configuration ($\theta_{\text{inc}}$ = -27.13° at 1520 nm) but this would



Downloaded From: https://www.spiedigitallibrary.org/conference-proceedings-of-spie on 07 Jun 2020
Terms of Use: https://www.spiedigitallibrary.org/terms-of-use

result in an angular scan of just 3.13°. Similarly, the $1/e^2$ horizontal beam diameter decreases with the increasing wavelength of the tunable source. For example, at 1600 nm the $1/e^2$ horizontal beam diameter (at 17 cm from the grating) is measured as 1.58 mm (which indicates an effective horizontal scanner aperture of 0.47 mm at 1600 nm; compare it with vertical scanner aperture of 8.6 mm that stays constant with wavelength of the tunable source). This indicates higher beam divergence in the scanning plane at higher wavelengths of the tunable source (e.g., 4.3 mrad at 1600 nm). The situation can be improved by reducing the wavelength range of the tunable source (e.g., from 1520 nm to 1580). As mentioned before, limiting the tunable bandwidth will decrease the angular scan range (to 8.68°). However by using smart design approaches (discussed in next section), significant angular scan range can be reached with minimum scanner insertion loss variation.

## 3. SMART W-MOS MODULES FOR WIDE ANGULAR SCANS

As mentioned earlier, the free-space W-MOS scan range depends on the angle of incidence [see Eq. (1)]. Fast switching of optical beam to set the angle of incidence on the diffraction grating can help achieve significant angular scan range as well as minimum scanner insertion loss variations. Figure 8 shows a combination of P-MOS and W-MOS to achieve large 1-D scans. A tunable laser is connected to a fiber collimator via a PC. The collimated beam passes through a M-bit P-MOS and hits a diffraction grating. The grating can be tilted to set the angle of incidence $\theta_{inc} = 0.0$ when the P-MOS is in OFF state. Now if the tunable laser is tuned from 1520 nm to 1600 nm, the scanner will provide a scan of 7.95°. As soon as the first scan is completed, the P-MOS can be turned ON to produce for instance an angular tilt for the angle of incidence to 2.0°. Now tuning the laser from 1520 nm to 1600 nm will produce a scan of 12.96°. Note that the overlap between the two scanned sectors will be 2.5°. The total angular scan achievable from the scanner module shown in Fig. 8 will be 18.43°.

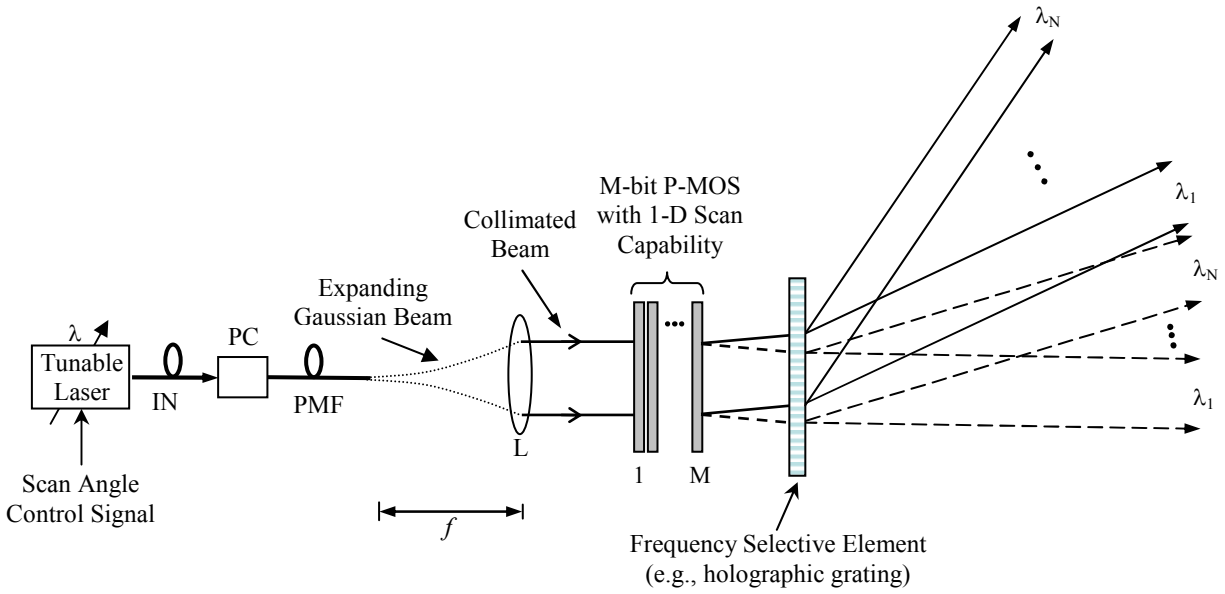


Fig. 8 shows a combination of the P-MOS and the free-space W-MOS to achieve large 1-D angular scans.

Figure 9 shows another scanner module that uses an acousto-optic (AO) deflector to adjust the angle of incidence on the diffraction grating in a free-space W-MOS. An AO deflector designed for 1550 nm has 1.76° Bragg angle (in air) when fed with a 100 MHz RF signal. Changing the frequency of the RF signal changes the period of the grating structure inside the AO Bragg cell, which in turn causes the diffracted beam to go under an angular displacement given by[16]

$$\theta_{out} = \sin^{-1}\left[\frac{\lambda f_a}{v_a} + \sin\theta_{inc}\right], \tag{7}$$



Downloaded From: https://www.spiedigitallibrary.org/conference-proceedings-of-spie on 07 Jun 2020
Terms of Use: https://www.spiedigitallibrary.org/terms-of-use

where $v_a$ is the speed of acoustic signal and $f_a$ is the frequency of the RF signal. An RF bandwidth of 40 MHz (around 100 MHz center frequency) implies 1.46° angular displacement in the first order diffracted beam. This fast (microsecond speed) optical beam switching capability of AO deflectors can be utilized to adjust the $\theta_{inc}$ on the diffraction grating in a free-space W-MOS to achieve wide 1-D angular scans.

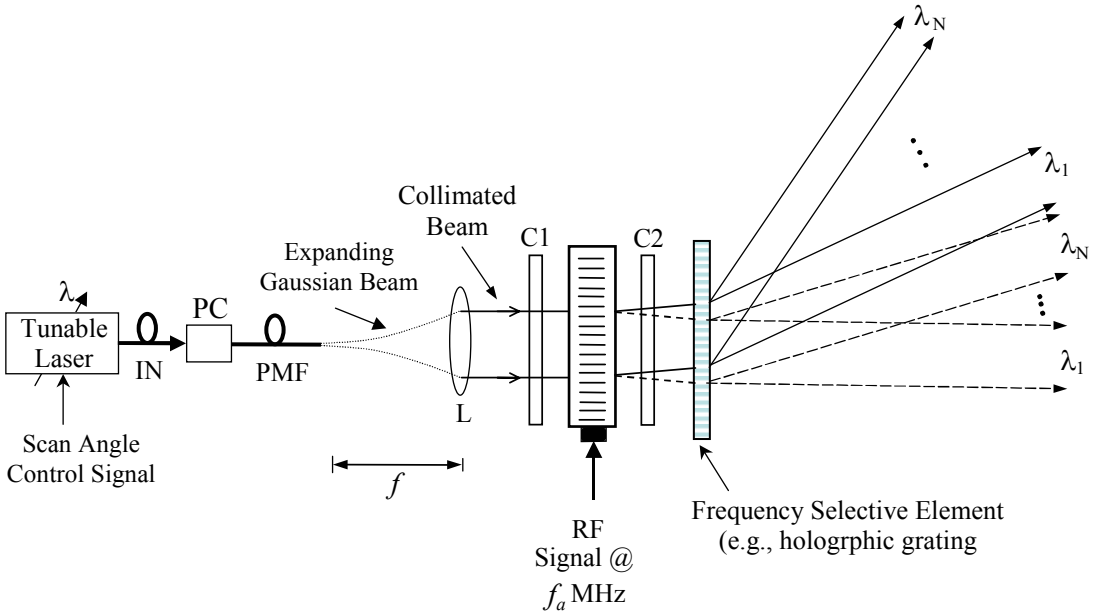


Fig. 9 shows a combination of the acousto-optic (AO) deflector and free-space W-MOS to achieve wide 1-D angular scans. C*i*: *i*th cylindrical lens.

Another approach to achieve wide 1-D angular scan range is shown in Fig. 10. A fast (μs speed) 1×2 fiber-coupled broadband optical switch is used to realize the scanner module. The two output fibers of the optical switch end up in an assembly that keeps the polished ends of the SMFs at one focal length distance from an achromatic lens. The two SMFs are parallel with each other such that one of the fibers is aligned with the principal axis of the lens whereas the other is shifted by $x'$.

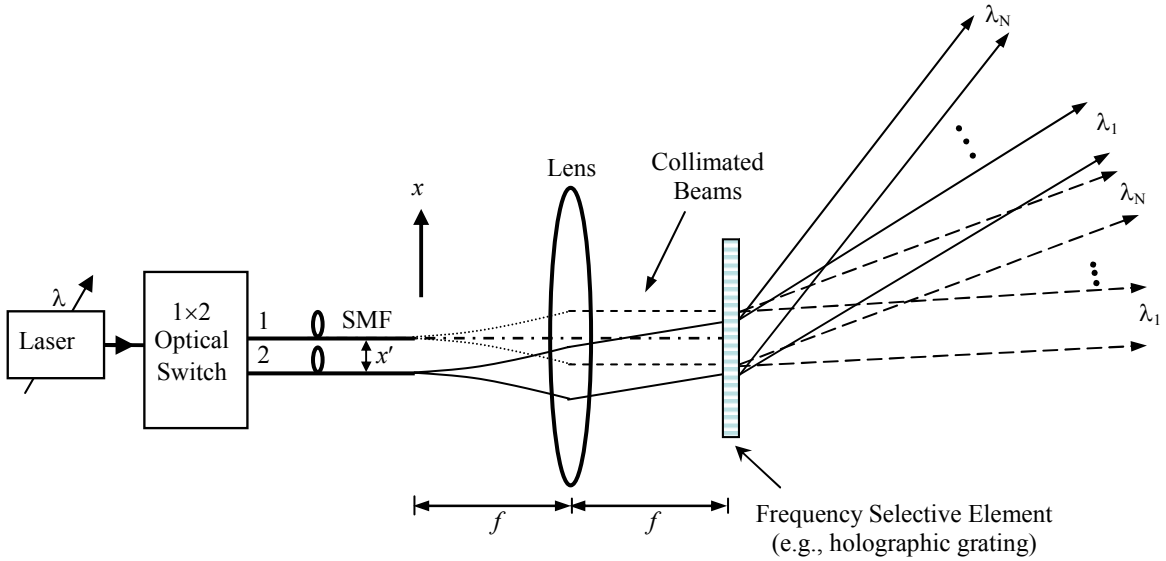


Fig. 10 shows a free-space W-MOS that uses a fast (μs speed) 1×2 optical switch to achieve wide 1-D angular scans.



Downloaded From: https://www.spiedigitallibrary.org/conference-proceedings-of-spie on 07 Jun 2020
Terms of Use: https://www.spiedigitallibrary.org/terms-of-use

The elevation angles and $1/e^2$ beam diameter (BD) of the collimated beams after the lens are given by

$$\theta' = -\tan^{-1}\left(\frac{x'}{f}\right) \tag{8}$$

and

$$1/e^2\,\mathrm{BD} = \frac{2\lambda f \cos\theta'}{\pi w_{\mathrm{inc}}}, \tag{9}$$

respectively, where $f$ is focal length of the collimating lens and $w_{\mathrm{inc}}$ is the beam waist of the Gaussian beam coming out of the SMFs. For instance, to set the angle of incidence $\theta_{\mathrm{inc}} = 2.0^{\mathrm{o}}$ in a smart W-MOS using $f = 45$ mm focal length lens, the SMF needs to be shifted by $x' = 0.524$ mm.

## 4. W-MOS MODULES WITH TWO-DIMENSIONAL ANGULAR SCAN CAPABILITIES

The design approaches discussed in the previous section can also be used to set skew incidence on the diffraction grating in a free-space W-MOS to achieve two-dimensional (2-D) angular scans.

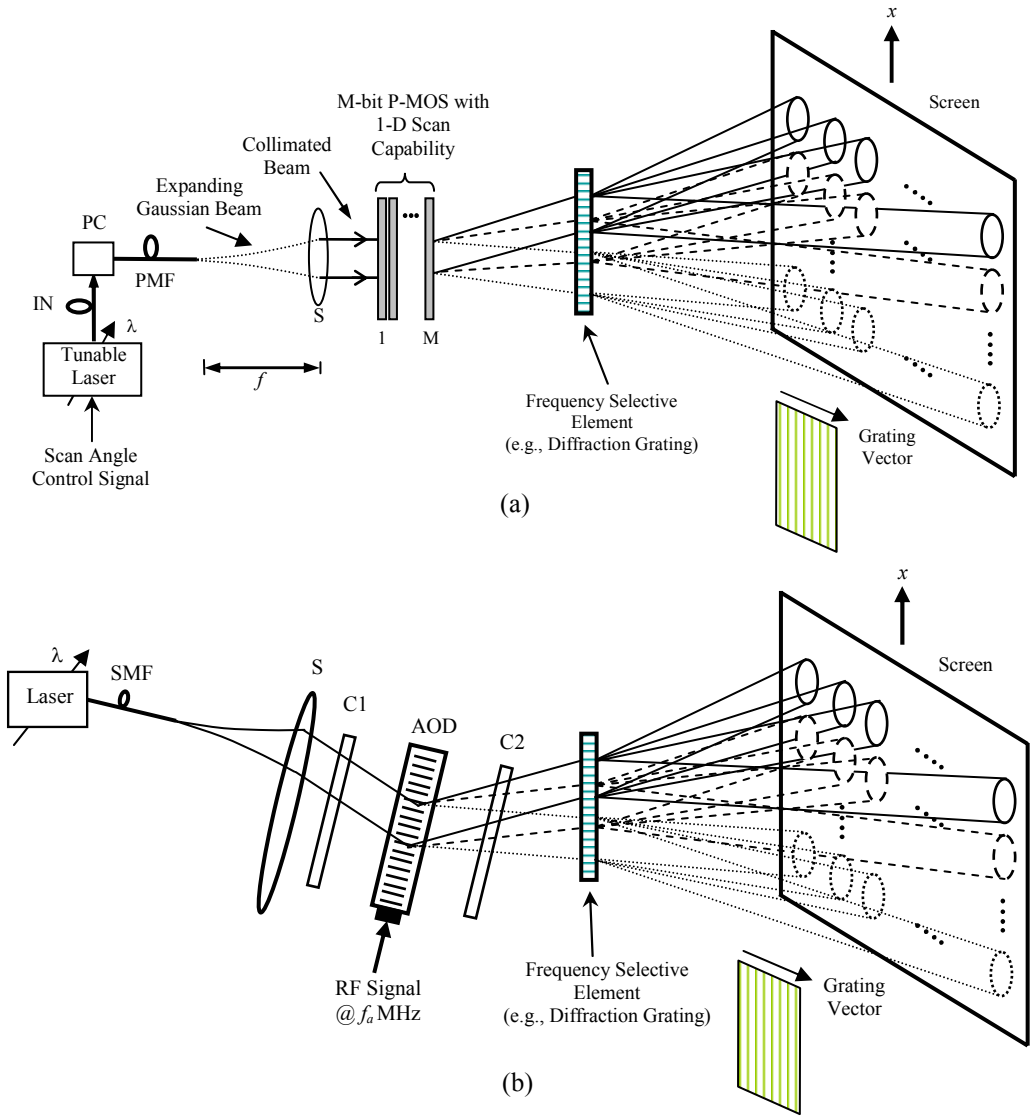


Fig. 11 shows integration of (a) P-MOS and (b) AO deflector in a free-space W-MOS for 2-D angular scans.



Downloaded From: https://www.spiedigitallibrary.org/conference-proceedings-of-spie on 07 Jun 2020
Terms of Use: https://www.spiedigitallibrary.org/terms-of-use

Figures 11 (a) and (b) show two schematics using a P-MOS and an AO deflector, respectively, to adjust the skew angle on the diffraction grating in a free-space W-MOS for fine elevation scans. Note that an elevation scan of 1° corresponds to 17.5 m displacement at 1 km distance. Figure 12 shows another schematic to achieve 2-D angular scans where the skew angle is adjusted using a 1×N optical switch. A P-MOS can also be introduced between the collimating lens and the diffraction grating to adjust the oblique angles on the grating as well and acquire wider angular scans along the *y*-axis along with fine elevation scans along the *x*-axis.

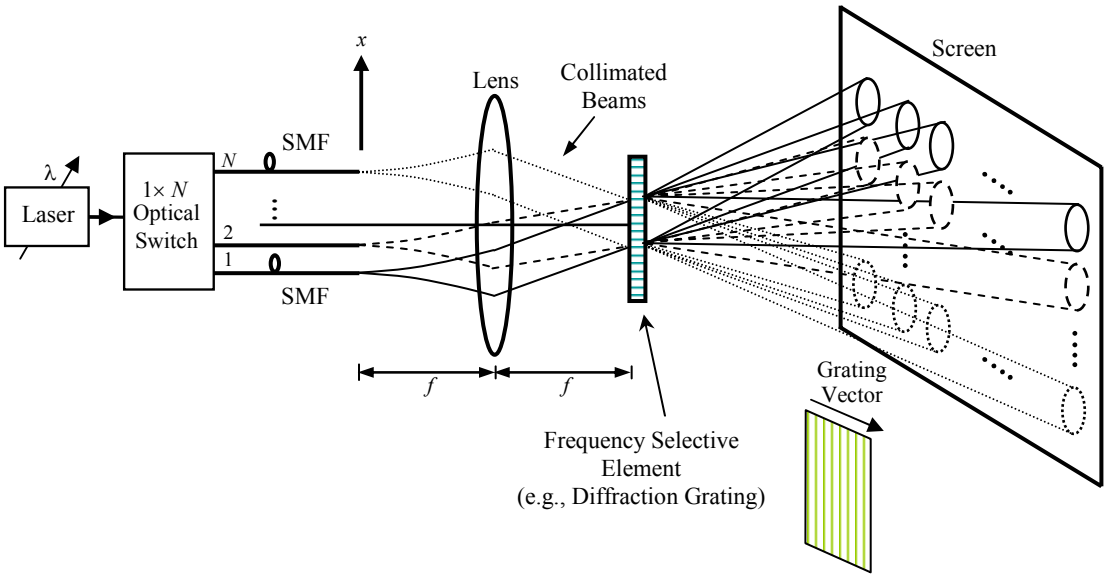


Fig. 12 shows a combination of AO deflector and free-space W-MOS for 2-D angular scans.

## 5. LASERCOM SUB-SYSTEM DESIGNS FOR 2π STERADIAN COVERAGE

Figure 13 shows the design of a transmit-receive lasercom sub-system for 360° azimuthal coverage with fine elevation scans. A tunable source is connected to a 1×N optical switch via a broadband circulator. Each of the output SMF from the switch goes to a front-end scanning head with M scan point capability. Each scanning head may feature 2-D wide angular scans as discussed in the previous section. Another option would be to use a MUX/DEMUX instead of an optical switch (after the circulator) and use P-MOS and/or S-MOS as the front-end scanning heads, for example. The same idea can be extended to realize an eye-safe transmit-receive lasercom sub-system with 2π steradian coverage for military mobile ground, air, and sea platforms (see Fig. 14).

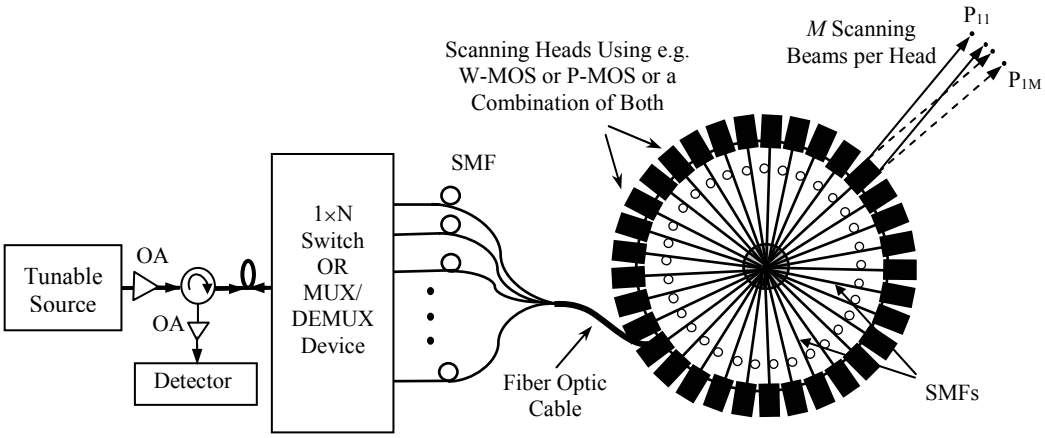


Fig. 13 shows a transmit-receive lasercom sub-system with 2π radians coverage and fine elevation scan capabilities.



Downloaded From: https://www.spiedigitallibrary.org/conference-proceedings-of-spie on 07 Jun 2020
Terms of Use: https://www.spiedigitallibrary.org/terms-of-use

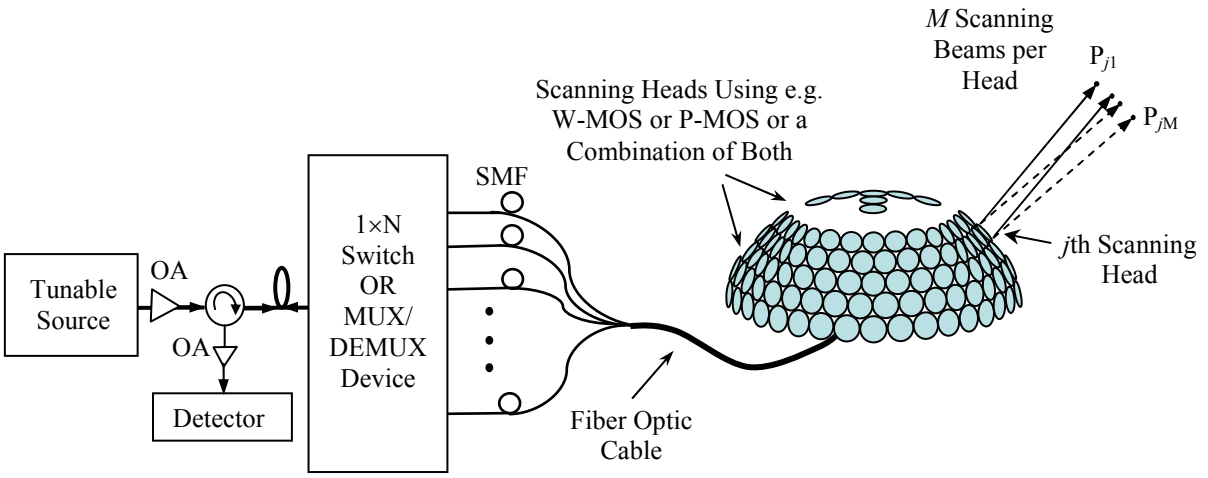


Fig. 14 shows a transmit-receive lasercom sub-system with 2π steradian coverage. OA: Optical Amplifier; SMF Single Mode Fiber; MUX/DEMUX: Multiplexer/Demultiplexer.

## 7. CONCLUSION

In conclusion, we have proposed novel architectures for wide area coverage agile optical scanning. The design and functionality of a hand-held free-space W-MOS unit is discussed. Experimental results attest to the simplicity of the W-MOS (using wavelength manipulations). In future, more compact free-space W-MOS designs will be realized using transmission diffraction gratings with high diffraction efficiencies. Using fast tunable lasers or optical filters, free-space W-MOS features microsecond domain scan setting speeds, single/multiple beam(s) in space, and large several centimeters or more diameter apertures for sub-degree angular scans. The potential speed of this fiber-optic scanning probe is in the GigaHertz rates using the present-day state-of-the-art nanosecond tuning speed lasers. In this paper, we introduced (for the first time) multiplexing at the scanner level to achieve wider scans per scanner module with fine elevation scan capabilities. The paper also proposes lasercom sub-system designs with $360^{o}$ azimuthal coverage with fine elevation scans and 2π steradian coverage for military mobile ground, air, and sea platforms.

## ACKNOWLEDGMENT

This work is partially supported by DARPA grant N66001-98-D-6003.

## REFERENCES

1. M. Gottlieb, C. L. M. Ireland, and J. M. Ley, "Electro-optic and acousto-optic scanning and deflection," Marcel Dekker (1983).
2. P. J. Talbot, Alder Creek, NY, "PLZT based electro-optic phased array optical scanner," U.S. Patent No. 5668657, Sep. 16, 1997.
3. M. E. Motamedi, S. Park, A. Wang, M. S. Dadkhah, A. P. Andrews, H. O. Marcy, M. Khoshnevisan, and A. E. Chiou, "Development of a micro-electro-mechanical optical scanner," Opt. Eng. **36**(5), 1346-1353 (1997).
4. W. Goltsos and M. Holtz, "Agile beam steering using binary optics microlens array," Opt. Eng. **29**(11), 1392-1397 (1990).
5. N. A. Riza, "MOST: Multiplexed optical scanner technology," in IEEE LEOS 13th Ann. Mtg. Conf. Proc. **2**, A. Weiner (ed.), IEEE Catalog No. 00CH37080, 828-829 (2000).
6. N. A. Riza and Y. Huang, "High speed optical scanner for multi-dimensional beam pointing and acquisition," in IEEE LEOS 12th Ann. Mtg. Conf. Proc. **1**, L. Goldberg (ed.), IEEE Catalog No. 99CH37009, 184-185 (1999).



Downloaded From: https://www.spiedigitallibrary.org/conference-proceedings-of-spie on 07 Jun 2020
Terms of Use: https://www.spiedigitallibrary.org/terms-of-use

7. Z. Yaqoob, A. A. Rizvi, and N. A. Riza, "Free-space wavelength-multiplexed optical scanner," Applied Optics, **40**(35), Dec. 10 (2001).
8. Z. Yaqoob and N. A. Riza, "Free-space wavelength-multiplexed optical scanner demonstration," Applied Optics, **41**(26), Sep. 10 (2002).
9. F. Delorme, G. Alibert, C. Ougier, S. Slempkes, and H. Nakajima, "Sampled-grating DBR lasers with 181 wavelengths over 44 nm and optimized power variation for WDM applications," in Opt. Fiber Commun. Technical Digest (OFC '98), 379-381 (1998).
10. N. A. Riza, "BOPSCAN technology: a methodology and implementation of the billion-point optical scanner," in International Optical Design Conference, L. R. Gardner and K. P. Thompson, ed(s)., Proc. SPIE 3482, Hawaii, June (1998).
11. Product No. NYW-50-001 (ADC Altitun, P.O. Box 911, SE - 175 29 Järfälla – Stockholm, Sweden, May 2000).
12. Product No. MTX-TEML (Multiplex Inc., Corporate Headquarters, 115 Corporate Blvd., South Plainfield, NJ 07080, U.S.A., November 2000).
13. I. C. Chang, "Progress of acousto-optic tunable filters," in IEEE Ultrasonics Symp. Proc. **2**, 819-825 (1996).
14. I. C. Chang, J. Xu, and D. Wo, "Bandpass response of collinear beam acousto-optic tunable filters," in IEEE Ultrasonics Symp. Proc. **1**, pp. 745-748 (1997).
15. A. Sneh, K.M. Johnson, "High-speed continuously tunable liquid crystal filter for WDM networks," IEEE Journal of Lightwave Technology, Vol. 14, No. 6, June 1996.
16. A. Yariv and P. Yeh, *Optical Waves in Crystals: Propagation and Control of Laser Radiation*, John Wiley & Sons, Inc., 1984.



Downloaded From: https://www.spiedigitallibrary.org/conference-proceedings-of-spie on 07 Jun 2020
Terms of Use: https://www.spiedigitallibrary.org/terms-of-use